Journal of Harbin Engineering University
ISSN: 1006-7043

Vol 45 No. 1
January 2024

Micro-Electrical Discharge Machining of Titanium Alloy (Ti-6Al-4V) Using Triangle Electrical Current Pulse Principle

K. Kalaiarasi [a], E. Kavitha [b], C.Senthilkumar [c], M. Balamururgan [d]

[a] Assistant Professor SG, Department of ECE, Saveetha School of Engineering, Saveetha Institute of Medical and Technical Sciences, India

[b] Assistant Professor SG, Department of IT, University College of Engineering villupuram, India

Assistant Professor SG, Department of Applied Electronics, Saveetha School of Engineering, Saveetha Institute of Medical and Technical Sciences, India

[c] Associate Professor, Department of Mechanical Engineering, University College of Engineering Panruti, India

[d] Associate Professor, Department of ECE, Saveetha School of Engineering, Saveetha Institute of Medical and Technical Sciences, India

Abstract

Titanium alloys are extensively used in the aviation, nano technology, solenoid valve, pharmaceutical industries and can be used in a variety of design-related sectors due to its unique material properties. Due to titanium alloy's poor heat flux, strong corrosiveness, and lower tensile flexibility in traditional machining, producing micro holes is a difficult process. To overcome these difficulties and produce micro holes with the highest level of dimensional precision and surface texture grade, Electric Discharge Machining (EDM) is a good option. Determining how various input variables, such as current, pulse on time with triangle wave, and pulse off time (TOFF), affect the machining capabilities of MRR and OC during the micro-EDM process is the aim of this work. For experimentation response surface methodology with face centered composite rotatable design were utilized and the output were recorded. Statistical analysis was used to establish the relationship between various technique factors and the micro-EDM efficiency process. ANOVA is used to ascertain the most significant variable. The various surface defects produced by the micro-EDM surface holes were examined using micrograph.

Keywords: Electrical discharge machining, Triangular current pulse, Material removal rate, Overcut.

1. Introduction

Aviation industry, electronics industry and medical sector need high strength, toughness and corrosive resistance material like Ti alloy. However, machining of micro-holes in Titanium alloys is a major challenging task using traditional machining methods, due to its greater hardness, sub surface damages such as metallurgical alterations, work hardening and micro cracks. Therefore, the preferred choice for creating micro-scale components with the highest possible level of dimensional precision and machined surface is electrical discharge machining (EDM). [1]. EDM operates according to the electro-thermal machining concept, which uses electrical energy to create an electrical discharge that is then transferred to heat energy without making physical contact between the work material and the electrode. The spark produces temperatures between 8,000°C to 15,0000°C, melting and evaporating the workpiece, therefore removal of molten metal from the surface of the material takes place [3]. Due of EDM's usefulness, the method has been scaled down to the micro level EDM .The modified form of electrical discharge machining technologies used to create micro- and small components and structures is known as micro-electrical discharge machining (-EDM). Similar to conventional EDM, micro-EDM removes material by repeatedly igniting an electric spark

between the tool and the surface of the material [4]. The dimension of the tool and the type of pulse generator employed are the two main differences between micro-EDM and standard EDM. When performing micro-EDM, the pulse generator creates very brief pulses with a pulse duration of a few microseconds or nanoseconds. [5]. Micro-EDM offers a high screen resolution, improved accuracy, and significant design flexibility with no physical pressure, jitter, or vibration in micro-sized holes. Because of the aforementioned benefits, micro-EDM is particularly effective in creating holes of any size, including blind holes with a 20:1 aspect ratio and microscopic dimension holes down to 10 mm [6]. Due to its unique features, titanium alloy can be machined using micro-EDM to produce rapid chilling holes in titanium alloys for aerospace propeller blades [7]. In a dry cooling environment, Lucia Lizzul et al. (2021) studied the microstructure alterations and wear resistance of Ti-6Al-4V ELI alloy. It was discovered that as the temperature in the cutting region rises, the top machined workpiece surface is damaged and the surface microstructure is altered. The roughness of the surface grew as the temperature increases [8]. Using a CVD coated insert, Amir Malakizadi et al. (2022) assessed the Ti-6al-4V ELI alloy's overall rating. It was discovered that the supply has a significant influence on the machining workpiece's surface quality. The machined surface was altered by changes in the microstructure and texture of the surface. A white layer with a thickness of 2µm was also observed during high-speed machining with a high feed rate [9].Various types of pulse shapes are used for machining, and these shapes have varying effects on how well the machining process performs. Consequently, it is anticipated that improving the percentage removal as the ratio of the quantity of debris to the amount of liquid metal will considerably boost the machining efficiency [10-11]. The cutting speed and wear rate are reportedly impacted by the discharge current pulse shape, according to prior studies. The rectangular current pulses have been employed extensively. If successful machining utilizing micro-EDM is necessary, it is imperative to properly choose the system parameters for a conservative manufacturing operation [12]. Li et al. observed that a rectangle waveform's computational time and cutting performance were excellent due to a high heat flow, but a triangular waveform's surface smoothness was better due to a reduced pulse time [13]. Mayu shinohara et al. (2020) looked into an LC pulse generator that could produce triangle discharge current pulse forms with a rapid rate of increase in speed. It was based on an inductive voltage boosting circuit. The results of this study showed that discharge current pulses with a limited duration and a quick rising speed can enhance the volume of a single discharge. These findings show that the LC pulse generator outperforms the RC generator in terms of machining efficiency and drilling accuracy at the same discharge frequency [14]., Using multiple emission current pulse formats with exponentially changing switching frequencies with pulse duration in various ways, Makarand M. et al. examined the machining performance, electrode geometry, and formation of pulse duration emission [15]. Although various current pulse has been employing EDM, triangular current pulse has not been documented in earlier publications, which confirms the uniqueness of this research. This study is significant because it examines how a triangle current pulse affects output variables like MRR and OC when Ti-6Al-4V alloy is machined using a micro electric discharge. To determine how multiple variables (current, pulse on time, and pulse off time) affected the output performance, a face-centered cubic design (FCCD) was used (MRR and OC). A component that fails to meet the required industrial standards for quality can be produced as a result of the impact of current pulse on machining processes. To get beyond these barriers and deliver the best results in the shortest amount of time, the micro EDM parameters must be tuned. Therefore, in order to fulfil process output goals like MRR maximization and OC minimization, appropriate variables must be defined. To get the maximum MRR and lowest OC, RSM was utilized to optimize the parameters. A JSM-6610LV Joel electron microscope from Japan was used to study the surface microstructure of the machined materials.

2.EXPERIMENTATION

Titanium alloys are widely used in manufacturing, due to light weight and superior mechanical properties. Due to its biocompatibility and effective combination of mechanical properties, Ti-6Al-4V is currently the most commonly utilized titanium-based material in the manufacture of medicinal elements, including dental implants, synthetic femoral parts and surgical tools. It consists of good machinability, suspension capacity and ductility. Titanium alloys do not corrode in the environment, such as freshwater, salt water and they are corrosion resistant even in organic acids. Titanium material (Ti-6Al-4V) was chosen as the wokpiece material with a dimension of 50mm x 35mm x 0.5mm has depicted in the Figure 1 before machining.

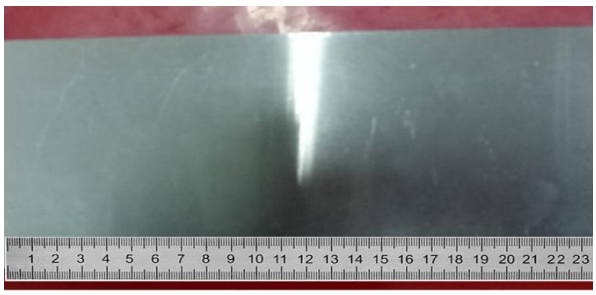

Figure 1. Titanium(Ti-6Al-4V) alloy before machining

2.1 CHARACTERISTICS OF Ti-6Al-4V ALLOY

Grade-5 titanium is the most popular titanium alloy, making up around 47% of the world's titanium production.

Table 1 Chemical Composition of Ti-6Al-4V

Al	C	Fe	H	N	O	Other	V	Ti
6	0.09	0.22	0.012	0.07	0.35	0.3	4.02	89.62

Table 2 Physical and Mechanical characteristics of Ti-6Al-4V

Physical characteristics	**Typical Value**
Hardness (g/cm^3)	5.02
Range of Melting (ºC±15 ºC)	1660
Specified Heating (J/kg°C)	570
Thermoelectric Permittivity (W/m K)	6.7
Tensile Strength (MPa)	876
Elastic Tension (GPa)	112
Mean Thermal Exp. Coeff. 0-100 (mm/mm-°C)	8.3 x 10^{-6}
Hardness Rockwell C	34

Whereas Ti-6Al-4V alloy is typically used in two metallurgical states such as annealed and weathered. In presence of heat removal rate and cutting force magnitude, raising temperature appears to be beneficial for machining titanium alloy. However, as the elastic modulus decreases, the workpiece deformation and vibration during milling become more fragile [16]. Tables 1 and 2 lists the chemical compositions, physical and mechanical properties of Ti-6Al-4V.

2.2 TOOL MATERIAL

A tubular copper wire was considered as the tool electrode with a diameter of 300µm because of its incredible thermal and mechanical properties as shown in Figure 2. Copper possess good electrical and thermal conductivity. Table 3 provides information about copper's physical characteristics.

Table 3 Physical characteristics of Copper

Material	**Cu**
Hardness (g cm^{-3})	8.96
Range of Melting ^{0}C	1084.62
Specified Heating (J/Kg K)	389
Thermoelectric Permittivity (W/mK)	390
Coefficient of thermal expansion (µm/m^{0}C)	15.7

Figure 2 Copper tool material

Figure 3 A

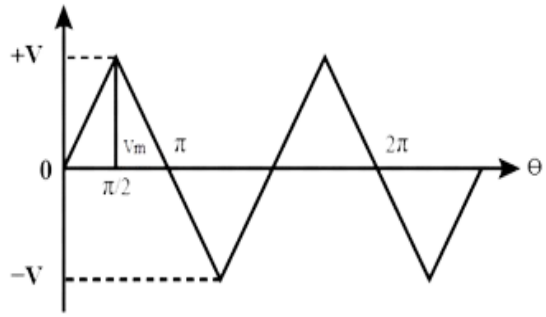

Figure 3 B

Figure 3 (a) Micro EDM machine,

(b) Triangular current pulse

MRR= work piece's initial weight –

$$\frac{\text{final weight after machining}}{\text{Machining process duration}} \quad (1)$$

OC= Actual dimension of Tool machining hole- Actual dimension of Tool

$$\frac{}{2} \quad (2)$$

We employed distilled water like an electrolyte solution and 3 axis controlled inter machining on the titanium alloy to perform a high accuracy micro machining operation. A transistor combination having 0.1 mm accuracy and a Triangle current pulse provided power for this device. The waveform is symmetrical about the voltage axis and repeats every two radians (360°). Alternating voltage and current, exhibit repetitivebehavior (AC). Here, a complete cycle is displayed. A Triangular wave's equation is as follows

$V=2/\pi\ V_m\theta$ for $0 \le \theta < \pi/2$

Where $V_m$is the median voltage,

Fig 3 (a) depicts the micro EDM machine and the triangular current pulse which is incorparted for machining. The MRR and OC have been calculated using the formulas 1 and 2.

The response surface methodology's goal is to create a statistical link between response and variables. This method aids in a better understanding of how changes in the application level of a series of variables affect response.

Experiments were carried out in accordance with a planned experiment based on a typical RSM design known as the central composite design. To acquire more data for modelling, the design required 20 trials encompassing the entire range of current, pulse on time and pulse off time. The parameters were assigned to the array using MINITAB statistical software version 17. During this phase, a total of 20 tests were carried out. Another crucial point is that, in order to reduce the effect of noise, all 20 trials were repeated three times in random order with the same set of machining variables. MRR and OC were used as response variables for this investigation. Table 4 depicts the Experimental Results of the Triangular Current Pulse.

Table 4 Experimental Results of the Triangular Current Pulse

S.No.	Current (Amp)	Pulse on time T_{ON} (µs)	Pulse off time T_{OFF} (µs)	MRR (mg/min)	OC (µm)
1	5	50	20	0.0239	49
2	9	50	20	0.0245	48
3	5	90	20	0.0263	47
4	9	90	20	0.0274	48
5	5	50	60	0.0232	46
6	9	50	60	0.0240	45
7	5	90	60	0.0268	49
8	9	90	60	0.0270	46

9	5	70	40	0.0259	40
10	9	70	40	0.0260	43
11	7	50	40	0.0245	44
12	7	90	40	0.0271	45
13	7	70	20	0.0262	47
14	7	70	60	0.0254	48
15	7	70	40	0.0260	46
16	7	70	40	0.0258	45
17	7	70	40	0.0259	43
18	7	70	40	0.0260	44
19	7	70	40	0.0256	42
20	7	70	40	0.0260	43

4 Result And Discussion

4.1 Modeling for Material Removal Rate

The results of ANOVA and quadratic model are shown in Table5 and Table6. The model's F value of 40.39 indicates that it is the most significant term. When a model's associated P value is smaller than 0.05 (95% confidence level), it is estimated that statistically significant. The typical F value percentage for a 95 percent confidence level is 4.06. The F value (4.04) for lack of fit is lesser than the typical value according to Table 5. The value of R^2 is 97.32% and the model creates a high-accuracy correlation between the input components and the MRR. For MRR the linear effect of current, T_{ON} and T_{OFF} are significant. The quadratic and interaction model are insignificant as observed from Table 6. The residuals for MRR are shown in a normal probability graph in Figure 4. If the faults are evenly distributed and the analytical prediction model accurately captures the observed data, the error terms will drop in a straight line. Equation 1 contains the final response equation for MRR.

MRR = 0.01600 + 0.000520 Current + 0.000138 T_{ON} + 0.000023 T_{OFF} - 0.000019 Current*Current- 0.000001 T_{ON}* T_{ON} - 0.000001 T_{OFF}* T_{OFF}- 0.000000 Current* T_{ON} - 0.000002 Current* T_{OFF} + 0.000000 T_{ON}* T_{OFF}

Table5 Estimation of Variance for MRR

Source	DF	Adj SS	Adj MS	F-Value	P-Value
Model	9	0.000024	0.000003	40.39	0.000
Linear	3	0.000022	0.000007	114.27	0.000
CURRENT	1	0.000001	0.000001	12.12	0.006
T_{ON}	1	0.000021	0.000021	325.11	0.000
T_{OFF}	1	0.000000	0.000000	5.58	0.040
Square	3	0.000001	0.000000	5.50	0.017
CURRENT*CURRENT	1	0.000000	0.000000	0.25	0.625
T_{ON}* T_{ON}	1	0.000000	0.000000	2.20	0.169
T_{OFF}* T_{OFF}	1	0.000000	0.000000	2.20	0.169
2-Way Interaction	3	0.000000	0.000000	1.41	0.296
CURRENT* T_{ON}	1	0.000000	0.000000	0.02	0.892
CURRENT* T_{OFF}	1	0.000000	0.000000	0.95	0.353
T_{ON}* T_{OFF}	1	0.000000	0.000000	3.27	0.101
Error	10	0.000001	0.000000		
Lack-of-Fit	5	0.000	0.000	4.04	0.07

		001	000		6
Pure Error	5	0.000 000	0.000 000		
Total	19	0.000 024			

Table 6 Analysis of Regression Coefficient for MRR

Term	Coef	SE Coef	T-Value	P-Value
Constant	0.025941	0.000087	296.73	0.000
CURRENT	0.000280	0.000080	3.48	0.006
T_{ON}	0.001450	0.000080	18.03	0.000
T_{OFF}	-0.000190	0.000080	-2.36	0.040
CURRENT*CURRENT	-0.000077	0.000153	-0.50	0.625
T_{ON} * T_{ON}	-0.000227	0.000153	-1.48	0.169
T_{OFF} * T_{OFF}	-0.000227	0.000153	-1.48	0.169
CURRENT* T_{ON}	-0.000013	0.000090	-0.14	0.892
CURRENT* T_{OFF}	-0.000087	0.000090	-0.97	0.353
T_{ON} * T_{OFF}	0.000163	0.000090	1.81	0.101

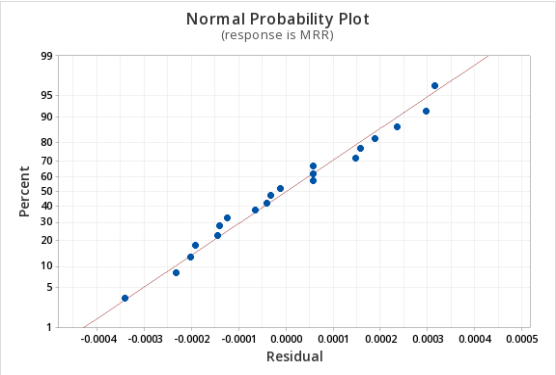

Figure 4 Normal probability plot Residual for MRR

4.2 Modeling for Overcut

For overcut, a similar technique is used, and the ANOVA results are provided in the Table 7 and quadratic model is depicted in Table 8. The model's F value, which is 4.51, shows that it is significant. The overall average value for the f distribution is 4.06 with a 95% confidence level. The F - ratio indicating an inadequate fit, as shown in Table 7, is 1.10, that is below the typical value. This makes the model vital. The model's accompanied p value is smaller than 0.05 (95% probability), demonstrating the model's validity. As depicted from the Table 8 the quadratic effect of T_{OFF} is the most significant factor. The model can account for 98.21% is quite close to 100%, which is a good sign. The residuals' standard probability graph for OC is shown in Figure 5. Because the error terms almost fall within the confidence interval, the linear regression is adequate and the errors are uniformly scattered. The functional relationship between input parameters and overcut are given in Equation 2.

OC =54.6 + 6.81 Current - 0.474 T_{ON} - 0.905 P_{OFF} - 0.455 Current*Current + 0.00295 T_{ON}* T_{ON} + 0.01045 T_{OFF}* T_{OFF} - 0.0000 Current* T_{ON} - 0.0125 Current* T_{OFF} + 0.00188 T_{ON}* T_{OFF}

Table 7 Estimation of Variance for OC

Source	DF	Adj SS	Adj MS	F-Value	P-Value
Model	9	92.091	10.2323	4.51	0.014
Linear	3	3.500	1.1667	0.51	0.682

Current	1	0.100	0.1000	0.04	0.838
T_{ON}	1	0.900	0.9000	0.40	0.543
T_{OFF}	1	2.500	2.5000	1.10	0.319
Square	3	82.091	27.3636	12.05	0.001
Current*Current	1	9.091	9.0909	4.00	0.073
T_{ON}* T_{ON}	1	3.841	3.8409	1.69	0.223
T_{OFF}* T_{OFF}	1	48.091	48.0909	21.18	0.001
2-Way Interaction	3	6.500	2.1667	0.95	0.451
Current* T_{ON}	1	0.000	0.0000	0.00	1.000
Current* T_{OFF}	1	2.000	2.0000	0.88	0.370
T_{ON}* T_{OFF}	1	4.500	4.5000	1.98	0.190
Error	10	22.709	2.2709		
Lack-of-Fit	5	11.876	2.3752	1.10	0.461
Pure Error	5	10.833	2.1667		
Total	19	114.800			

Table 8 Estimated Regression Coefficient for OC

Term	**Coef**	**SE Coef**	**T-Value**	**P-Value**
Constant	43.627	0.518	84.21	0.000
Current	-0.100	0.477	-0.21	0.838
T_{ON}	0.300	0.477	0.63	0.543
T_{OFF}	-0.500	0.477	-1.05	0.319
Current*Current	-1.818	0.909	-2.00	0.073
T_{ON} * T_{ON}	1.182	0.909	1.30	0.223
T_{OFF} * T_{OFF}	4.182	0.909	4.60	0.001
Current* T_{ON}	-0.000	0.533	-0.00	1.000
Current* T_{OFF}	-0.500	0.533	-0.94	0.370
T_{ON} * T_{OFF}	0.750	0.533	1.41	0.190

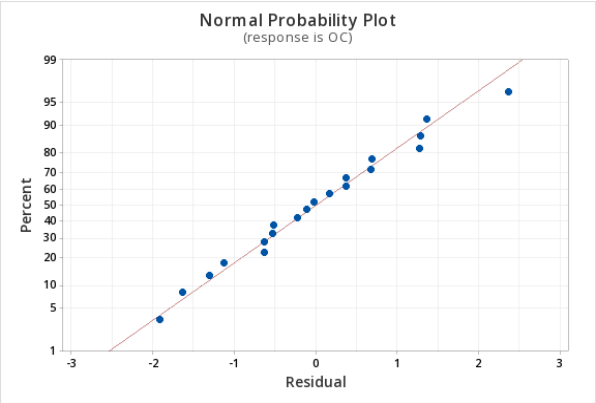

Figure 5 Normal probability plot Residual for OC

4.3 MICRO EDM CHARACTERISTICS ON TRIANGULAR CURRENT PULSE

A highly reinforced plasma channel is created by the triangular pulse, which has a peak during the early part of the pulse period, which accelerates the melting of the electrodes during the discharge. The development and expansion rates of the plasma channel are slowed by a decrease in the peak at the first and last parts of the pulse period. The liquid film explodes uniformly as a result of the pulse length's peak's drop, which helps to continuously remove more material from the electrodes. The following are the impact of process factors on performance attributes during triangular current pulse machining.

4.4 Influence of control variable on MRR

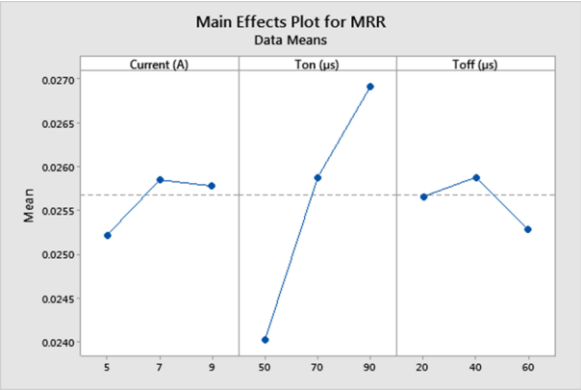

Figure 6 Influence of current and pulse on time on MRR

Figure 6 illustrates how the MRR rises as the current and period of pulse increases. MRR is high at low current settings (6 to 7.5 amps), however as current is raised to 9 amps, MRR starts to decline. It can be observed that in triangular waveform current gradually increases from 6 to 9 amps which implies that discharge electron beam width from cathode continuously rises. Therefore, the heat transferred to the workpiece surface is uniform, cause high-intensity sparks [17]. This high intensity spark results in frequent melting and vaporization of workpiece along with high removal of material [18]. The time consumed by peak current (9 amp) is minimum. Because there is no steady current supplied during triangular wave. When current falls, intensity of electron beam width reduced. Therefore, poor discharge spark intensity and enlargement of the liquid film are reduced by stepping down the peak during the second half of the pulse length [19]. As a result, each discharge results in a gentle removal of molten material, resulting in a stable machining process with many pores is depicted in Figure 7. It has been demonstrated that discharge energy increases as pulse on time rises from 60 to 75µ seconds. Once an appropriately emission current is assigned, the transfer rate of heat can continue to be significant enough to release the liquid metal within the debris field despite the spark thermal radius expands so at end of emission to extract the substance from the huge liquid metal due to hopping. Moreover, increasing the pulse on time to 90µs causes the spark plasma width to become wide at the commencement of discharge, which considerably increases removal due to the high thermal gradient. Results in the highest removal quantity of MRR because the heat transfer rate is high enough at the discharge's termination. Further, molten material to be driven out from the workpiece with higher formation of uneven globules and pockmarks [20] as depicted in Figure 8.

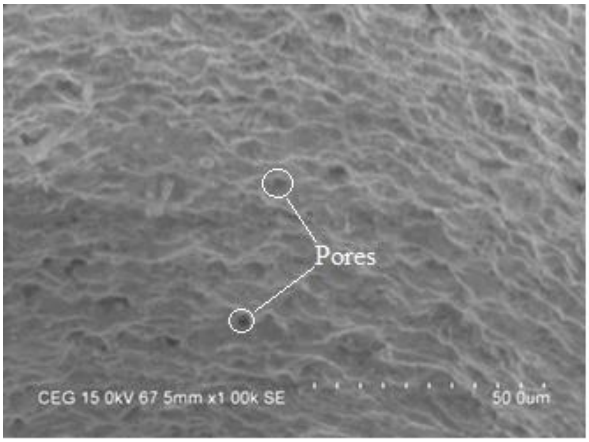

Figure 7 Pores at high current

The MRR increased with increasing current at all levels of pulse off time duration, as illustrated by the response surface plot in Figure 6. Efficient machining occurs in low pulse off time (20µs to 40µs). This is due to the that effective machining happens as sparking efficiency improves, and debris evacuated swiftly from the gap, and fresh dielectric fluid is injected, resulting in a higher MRR. On further increasing the off time duration from 40µs to 60µs the dimension of plasma channel reduces on the workpiece. Further, the number of sparks intruding on the surface in a particular time is reduced, leads to lower MRR and crater developed becomes shrinks as small voids on the machined surface seen in figure 9.

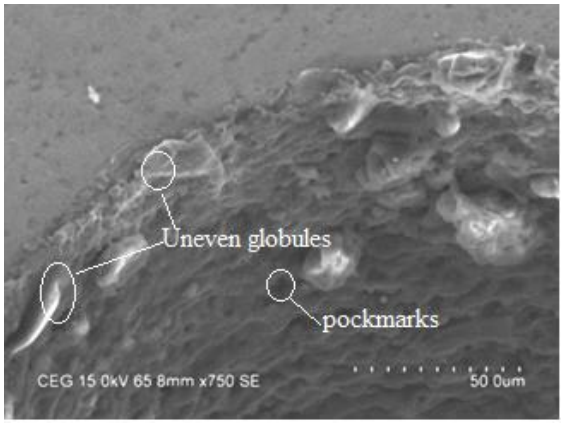

Figure 8 Uneven globules and pockmarks at higher pulse on time

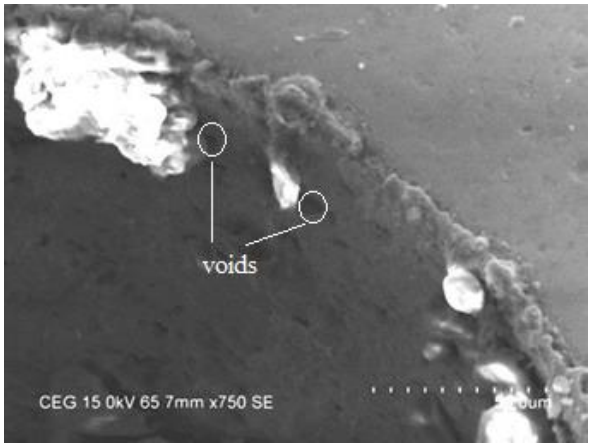

Figure 9 Voids formation at lower pulse off time

4.5 Influence of control variable on OC

The variations in overcut with regard to current, pulse on time and pulse off time are depicted in Figure 10. When current increases from 6 to 7.5 amps OC increases, further increase the current up to 9 amps overcut decreases.

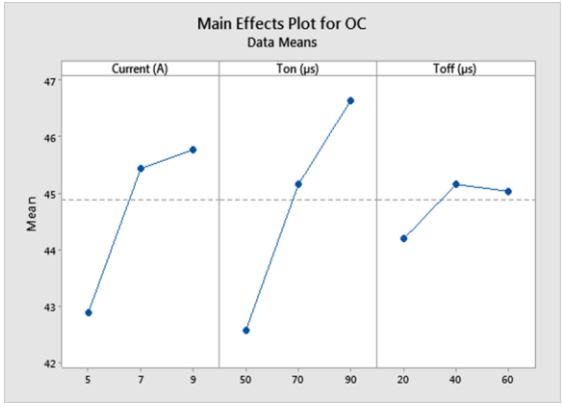

Figure 10 Influence of current and pulse on time on OC

It is observed that at low current of 6 amps, quick deterioration of the electrode material and the observed uncontrolled metal transfer on the surface occurs therefore OC increases As a result, the formation of globules is seen, as illustrated in Figure 11[21]. At higher current of 9 amps, thin and uniform plasma formation has been observed. This could be as a result of the strength of the discharge, which removes material from the workpiece leaving pores with wider craters on the surface, as seen in Figure 12. It is inferred that in triangular pulse deeper overcut was observed. During the pulse on time of 60µs a smaller vapour bubble is formed with a reduced power intensity which consumes less quantity of material resulting in a lower OC [22]. The energy imposed on the work piece surface increases once the pulse on time is extended from 60µs to 90µs. During the discharge, the ionized pathway and the vapour bubble surrounding it are increased, which has an effect on the growth in OC. The raise of pulse on time from 70µs to 90µs, surface of the workpiece melts and evaporates quickly therefore large concentration of high emission produced in the spark discharge gap which causes a substantial increase in OC. As shown in Figure 12, this leads the surface of the workpiece to develop larger craters and voids.

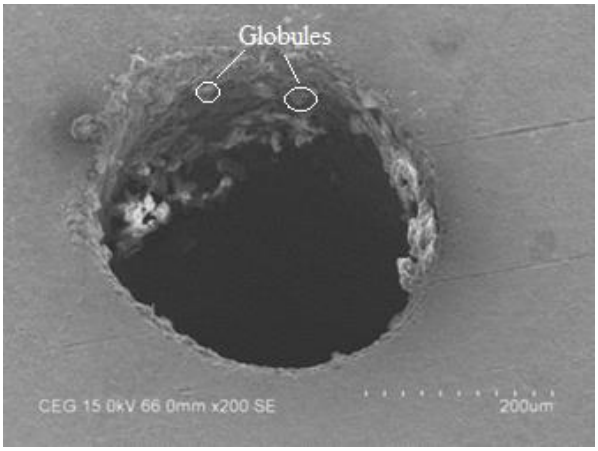

Figure 11 Globules formation at deeper current

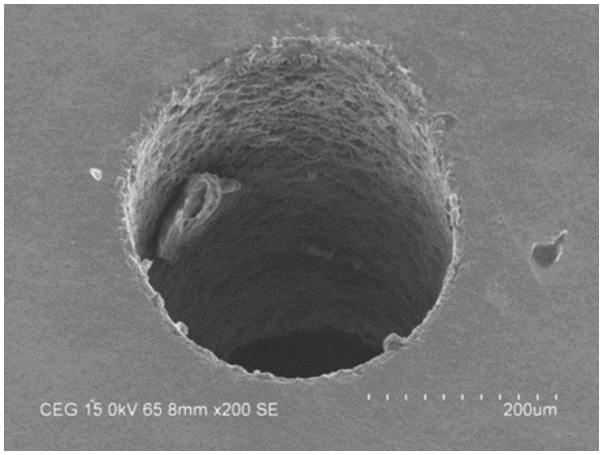

Figure12 Cavities and deeper craters at higher pulse on time

The relationship between current, pulse off time, and OC is shown in Figure 10. As the pulse off time extended from 20 to 40 µs, the ionized path created was shorter and only produced a little amount of ignited power that impacted on the surface and reduced the OC. The OC dramatically increases when the pulse off time is raised from 40 to 60 µs because the evacuation of debris during this period deteriorate the side wall of the cylindrical surface increases OC. The collision of electron beam width is greatly increased when the current is increased from 6 to 7.5 amps, and as a result, OC increases. Due to the high current, debris frequently solidifies on the edges of the surface as seen in Figure 13. On further increasing the current to 7.5 to 9 amps OC decreases [4]. Because reduced current emission is unstable in this situation, increasing the temperature in the inter electrode gap is inadequate to adequately emulsify the workpiece.

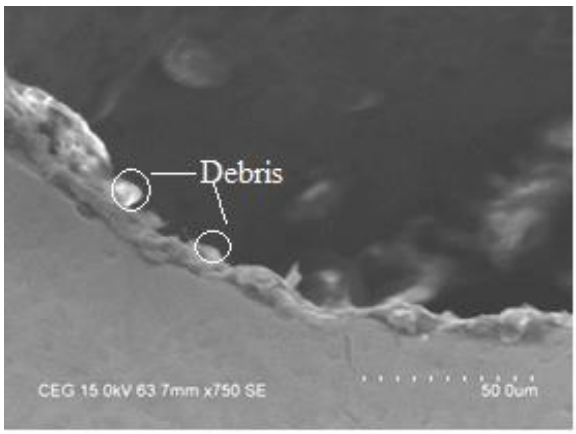

Figure 13 Debris formation at the edges for higher pulse off time

5 Optimization of Micro EDM Characteristics on Triangular Current Pulse

Figure 14 depicts the optimization plot for removal of material and overcut. The goal of this approach was to maximize MRR while lowering OC. The optimum values obtained from the graph are MRR= 0.0264 gm/min and OC = 41.7776 µm and the relevant parameters current (I), pulse on time (T_{ON}) and pulse off time (T_{OFF}) are 9A, 73.83µs and 41.01µs respectively. The desirability of optimization was calculated to be 0.9499, indicating that each parameter is within its acceptable range. Table 9 shows the verification of the test results for Material Removal Rate (MRR) and Overcut (OC) at the selected optimum circumstances. A strong correlation between the predicted and observed machining efficiencies was found after comparing the two outcomes. The error for material removal rate and overcut are 1.13 % and 3.57%, respectively, which is less than the allowable limit. This confirms the outstanding reproducibility of the experimental results.

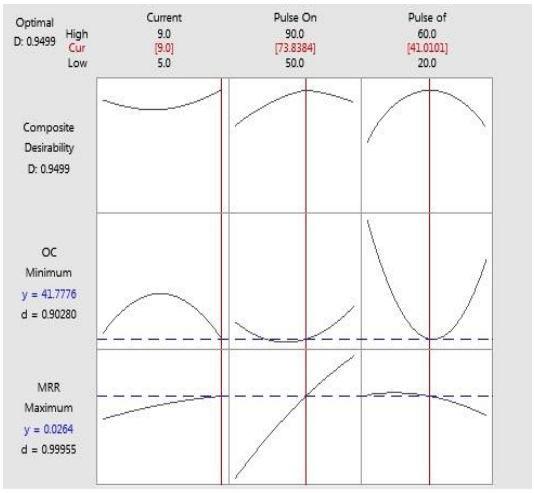

Figure 14 Optimal plot obtained through RSM for Triangular current pulse

Table 9 Validation test result for Triangular current pulse

S. No	Current (A)	T_{ON} (µs)	T_{OFF} (µs)	MRR			OC		
				Predicted	Actual	Error%	Predicted	Actual	Error %
1	9	73.83	41.01	0.0264	0.0267	1.13	41.777	40.284	3.57

6. Conclusion

In the current work, the efficacy of micro-EDM on a titanium alloy was evaluated. Analytical models were generated after an investigation of the effects of MRR and OC. The ANOVA's findings demonstrate the suitability of the developed models. Graphs for a number of micro electrical discharge machining parameters are also shown for the overall efficiency. According to the data, MRR increases as pulse-on time and current rise. The work material's rapid melting and evaporation could be explained by the fact that more heat is generated and held at a higher level for longer periods of time. The liquid film formation in Triangular pulse is high which causes uniform implosion of the plasma channel therefore aids in the controlled removal of additional molten metal. As a result, this pulse form ranks best among to obtain high MRR. It is inferred that in triangular pulse, the ionized pathway and energy discharge is higher causes deeper overcut. Response surface methodology was used to carry out the optimization. It was found that there was a good agreement between the predicted and actual machining performance when the expected and actual machining performance were compared and it was found that error was within the permissible limit.

References

1. Jingwei Zhao, Zhengyi Jiang, Leszek A. Dobrzański, Chong Soo Lee, and Fuxiao Yu. Recent Development in Micro manufacturing of Metallic Materials, Materials (Basel). 2020 Sep; 13(18): 4046. doi: 10.3390/ma13184046.
2. Asif Rashid and Muhammad P. Jahan. Microfabrication by electrical discharge machining-based hybrid processes, Micro Electro-Fabrication, Micro and Nano Technologies, 2021, Pages 33-62. https://doi.org/10.1016/B978-0-12-820049-0.00008-6
3. AsfanaBanu& Mohammad Yeakub Ali 2016, 'Electrical Discharge Machining (EDM): A Review', International Journal of Engineering Materials and Manufacture, vol. 1, no. 1, pp. 3-10.
4. Asarudheen Abdudeen ,Jaber E. Abu Qudeiri , Ansar Kareem, ThanveerAhammed and AimanZiout. Recent Advances and Perceptive Insights into Powder-Mixed Dielectric Fluid of EDM, Micromachines 2020, 11, 754; doi:10.3390/mi11080754.
5. Dong Yang and Zhanqiang Liu. Quantification of Microstructural Features and Prediction of Mechanical Properties of a Dual-Phase Ti-6Al-4V Alloy, Materials (Basel). 2016 Aug; 9(8): 628. doi: 10.3390/ma9080628.
6. Rajusing Rathod, Dinesh Kamble & Nitin Ambhore. Performance evaluation of electric discharge machining of titanium alloy-a review. Journal of Engineering and Applied Science volume 69, Article number: 64 (2022). https://doi.org/10.1186/s44147-022-00118-z.
7. Ziliang Zhu, DengjiGuo, Jiao Xu, Jianjun Lin,Jianguo Lei, Bin Xu, Xiaoyu Wu, and Xujin Wang. Processing Characteristics of Micro Electrical Discharge Machining for Surface Modification of TiNi Shape Memory Alloys Using a TiC Powder Dielectric, Micromachines (Basel). 2020 Nov; 11(11): 1018. doi: 10.3390/mi11111018.
8. LuciaLizzuL, Marco Sorgato, Rachele Bertolini, Andrea Ghiotti and Stefania Bruschi 2021. Anisotropy effect on Laser Powder Bed Fused Ti6Al4V machinability, Procedia CIRP, Volume 101, 2021, Pages 30-33.
9. Amir Malakizadi, Dinesh Mallipeddi, Sasan Dadbakhsh, Rachid M'Saoubi & Peter Krajnik 2022, 'Post-processing of additively manufactured metallic alloys - A review', International Journal of Machine Tools and Manufacture, vol. 179, 103908
10. Mayushinahara& Masanori kunieda. Influences of discharge current pulse shape on machining characteristics in EDM, procedia CIRP 95 (2020) 200-203. Doi:10.1016/j.procir.2020.03.146
11. Valeria Marrocco, Francesco Modica, Vincenzo Bellantone, Valentina Medri, and Irene Fassi, Pulse-Type Influence on the Micro-EDM Milling Machinability of Si_3N_4–TiNWorkpiecesMicromachines

(Basel). 2020 Oct; 11(10): 932. doi: 10.3390/mi11100932**.**

12. K. Kalaiarasi, C. Senthilkumar, M. Balamurugan, R. ArokiaDass. Micro-electrical discharge machining of Titanium alloy (Ti-6Al4V) by Sawtooth pulse current, Int. J. Electrochem. Sci., 17 (2022) Article Number: 220442, doi: 10.20964/2022.04.41.
13. C. J. Li, J. J. Ding, S. Q. Yang, Y. S. Fang & Q. C. Kong. Discharge current shape control method and experiment in wire EDM, The International Journal of Advanced Manufacturing Technology volume 87, pages3271–3278 (2016)
14. Mayu Shinoharaa & Masanori Kuniedaa 2020, 'Influences of discharge current pulse shape on machining characteristics in EDM', Procedia CIRP, vol. 95, pp. 200-203.
15. Makarand M. Kane, AjinkyaAjitPhanse, Himanshu J. Bahirat, S.V. Kulkarni. Classification and comparative study of EDMpulse generators, IET Power Electron., 2020, Vol. 13 Iss. 14, pp. 2943-2959.
16. Gangireddy & Mates, S 2017, 'High Temperature Dynamic Response of a Ti-6Al-4V Alloy: A Modified Constitutive Model for Gradual Phase Transformation', Journal of Dynamic Behavior of Materials, vol. 3, pp. 557-574.
17. Debabrata Datta 2021. Thermal Analysis of a Workpiece Material in an Electric Discharge Process, Evolutions in Mechanical Engineering, Volume3 Issue4, DOI: 10.31031/EME.2021.03.000569
18. Ayanesh Y Joshi & Anand Y Joshi 2019, 'A systematic review on powder mixed electrical discharge machining', Heliyon, vol. 5, issue 12, e02963.
19. Azat Bilal, Muhammad Pervej Jahan, Didier Talamona and Asma Perveen 2019. Electro-Discharge Machining of Ceramics: A Review, Micromachines 2019, 10(1), 10 https://doi.org/10.3390/mi10010010.
20. Elaiyarasan U, V Satheeshkumar and C Senthilkumar 2018. Experimental analysis of electrical discharge coating characteristics of magnesium alloy using response surface methodology, Materials Research Express, Volume 5, Number 8, DOI 10.1088/2053-1591/aad11f
21. Santosh Kumar Yadav, Abhishek Singh & Kishore Debnath 2022, 'Experimental study of hole overcut and taper during Electrochemical Discharge Machining (ECDM) of CFRP composite', Materials Today Proceeding, vol. 59, pp. 1054-1058.
22. Kashif Ishfaq, Muhammad Asad Maqsood, Saqib Anwar, Abdullah Alfaify & Abdul Wasy Zia, 2022. Analyzing micromachining errors in EDM of Inconel 600 using various biodegradable dielectrics, Journal of the Brazilian Society of Mechanical Sciences and Engineering volume 44, Article number: 249 (2022).